Groundwater for Sustainable Development 29 (2025) 101427

Contents lists available at ScienceDirect

Groundwater for Sustainable Development

journal homepage: www.elsevier.com/locate/gsd

Research paper

Assessing the effects of ENSO-induced climate variability on shallow coastal groundwater reserves of north Patagonia, Argentina

Mattia Gaiolini [a], Rosario Acosta [b], Eleonora Carol [b], Nicolò Colombani [a,*]

[a] Department of Materials, Environmental Sciences and Urban Planning (SIMAU), Polytechnic University of Marche, 60131, Ancona, Italy
[b] Centro de Investigaciones Geológicas (CIG), Consejo Nacional de Investigaciones Científicas y Técnicas (CONICET), Universidad Nacional de La Plata (UNLP), La Plata, Argentina

HIGHLIGHTS

- A 3D numerical flow model estimate groundwater flows changes over 56 years period.
- The statistical correlation showed positive association among GW levels ONI and SPEI.
- Increasing seawater inflow was inferred due to decreasing meteoric recharge.

GRAPHICAL ABSTRACT

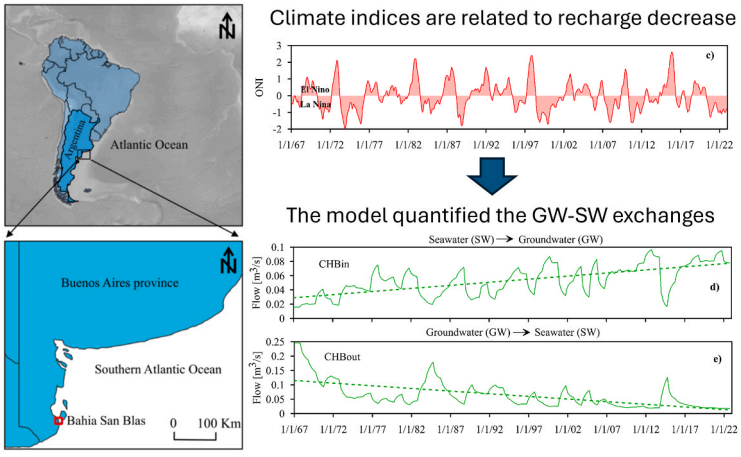

ARTICLE INFO

Keywords:
Coastal aquifer
Groundwater flow model
Hydrogeological budget
Climate change

ABSTRACT

In this study, a statistical correlation analysis, integrating climatic indices and numerically calculated hydrological datasets, was used to assess the impact of climate patterns and meteorological variability (identified by ONI and SPEI, respectively) on a coastal aquifer in a semi-arid area of Patagonia. To estimate aquifer groundwater levels and flows changes over the 56 years period (1967–2022) under analysis, a 3D numerical flow model was implemented, calibrated against observed piezometric heads and validated using remote sensing data from the GRACE mission. Results highlighted the role of meteoric recharge and evapotranspiration in shaping the water budget, highly affecting the piezometric fluctuation over the simulation. The statistical correlation showed a weak positive association between GW levels and both ONI and SPEI, indicating that climate and meteorological variability are exerting a slight but noticeable influence on groundwater dynamics. Moreover, an increasing seawater inflow from the ocean and tidal channels was observed due to decreasing meteoric recharge and this climate change-driven shift in water exchange dynamics could potentially increase salinization risk in the low-lying areas of this coastal aquifer. The developed methodology could help a proper water resource

* Corresponding author.
E-mail address: n.colombani@univpm.it (N. Colombani).

https://doi.org/10.1016/j.gsd.2025.101427
Received 3 October 2024; Received in revised form 30 January 2025; Accepted 16 February 2025
Available online 17 February 2025

management in a coastal region where groundwater is the only source of supply for residents, providing useful information for studying groundwater resources in other coastal areas of Patagonia and the world that face similar water problems.

1. Introduction

Freshwater resources are essential for sustaining life and their availability is increasingly threatened by numerous factors globally (Kumar, 2012; Bănăduc et al., 2022; Mishra, 2023). Climate change (CC) impacts, such as reduced meteoric precipitation, increasing temperatures and sea level rise are significantly altering the global hydrological cycle, with profound effects on groundwater (GW) systems (Oude Essink et al., 2010; Ferguson and Gleeson, 2012). Particularly, arid and semi-arid coastal areas are highly vulnerable to environmental changes exacerbated by the ongoing CC (Amanambu et al., 2020; Mastrocicco and Colombani, 2021). In these regions, surface water resources are often scarce and highly unreliable, making GW the primary source of freshwater to supports economic activities, such as agriculture and food production (Foster et al., 2013; Malki et al., 2017), and to maintain ecosystem services (Scanlon et al., 2006; Saito et al., 2021). Climatic fluctuations, combined with a growing water demand for drinking and irrigation purposes, are inducing a huge pressure on this already scarce water resources, further deteriorating both their quantity and quality (Srivastav et al., 2021).

The Argentine Patagonia region is one of the extratropical regions most affected by periodic climatic phenomena (Compagnucci and Araneo, 2007; Scordo et al., 2018). Freshwater resources availability along the coast of Argentine Patagonia are scarce, with few localities able to supply themselves through local exploitation of GW.

El Niño/Southern Oscillation (ENSO) represents the most important coupled ocean-atmosphere phenomenon driving global climate variability on interannual time scales (Yang et al., 2018). In the last decades, various studies associated precipitation anomalies recorded at different temporal scales in Patagonia to El Niño (EN) and La Niña (LN) phases of ENSO (Vargas et al., 1999, 2002; Grimm et al., 2000; Kayano and Andreoli, 2007).

Most of the existing research is focused on the ENSO effect on aboveground components of the hydrological cycle (e.g. precipitation anomalies, snow accumulation), while scientific knowledge on the subsurface component's sensitivity to EN climatic oscillation has been only recently emerging in literature (Piacentini et al., 2024; Navarro Céspedes et al., 2024; Joshi and Kalra, 2021, among others).

Other researchers used different indices and methodology to estimate the effect of climate variations on GW levels: as an example, Mercau et al. (2016) assessed climate, topography and crop effects on water table level dynamics in the Western Pampas; while Kuss and Gurdak (2014) investigated GW level response in U.S. principal aquifers to ENSO and others climate indices. These climate variations coupled with land use and land cover changes are among the main drivers of groundwater storage globally (Dasgupta and Sanyal, 2022), which in turns affect the water resources management (Scanlon et al., 2023).

The integration of hydrological datasets with climatic indices, such as Oceanic Niño Index (ONI), is pivotal for predicting how ENSO oscillation influence GW resources. Though, the availability of continuous datasets able to capture long-term changes in hydrogeological systems is a major challenge.

In this framework, GW numerical modelling offers an effective solution to develop a reliable and physically based representation of the subsurface system able to estimate GW table oscillation, flow dynamics and water budgets over extended periods. Since its release in 1988, MODFLOW has become the global standard for GW modelling due to its flexible modular structure, complete coverage of hydrogeological processes, and open accessibility (Zhou and Li, 2011).

In this study a 3D numerical flow model of Bahia San Blas coastal aquifer, in the Northern Patagonian coast (Argentina), was developed to estimate the interplay among climatic variations, meteoric forcings and GW fluctuations over a 56-year period (1967–2022). MODFLOW-NWT code (Niswonger et al., 2011), integrated within the new graphical interface PMWIN 11 (Chiang, 2022), was used to set up the flow model. A fully transient simulation on a sub-yearly (seasonal) basis was performed to analyze hydrologic regime at the aquifer scale. Changes in shallow GW reserves due to variations in precipitation associated with EN and LN events were assessed via statistical correlation analysis. To achieve this goal, historical and remote sensed datasets were utilized to inform the GW flow model.

Understanding how the interannual climate variability associated with ENSO influence hydrogeological regime at the aquifer scale is pivotal for achieving sustainable water resources management in response to CC-driven stressors. Especially, in regions most vulnerable to climate variability, this knowledge is needed to guide water policy and adaptive strategies.

2. Materials and methods

2.1. Hydrogeological characterization of the study area

The region is characterized by the absence of permanent river courses and the predominance of aquifers with high-salinity groundwater, which limits the availability of water sources suitable for human supply. However, hydrogeological environments with low-salinity water are present, typically associated with permeable beach ridges deposits, where rainwater infiltrates and is stored underground as freshwater lenses (Carol et al., 2021). Nevertheless, the arid climate of the area, where the average annual precipitation is close to 200 mm and the annual potential evapotranspiration is 730 mm (Misseri et al., 2020), places the aquifers under naturally severe water deficit conditions. Beach ridges that are separated by marsh and intertidal plain environments associated with the Jabali tidal channel, may be grouped according to different transgressive episodes (Rostami et al., 2000; Pedoja et al., 2011; Isla, 2017). The continental ones are associated with an ancient Pleistocene shoreline, while those located between the channel and the sea correspond to a Holocene shoreline that is currently active (Rutter et al., 1990; Fucks et al., 2012). Pleistocene ridges comprise a prevailing N-S oriented deposits reaching elevations of about 12 m a.s.l., while in more depressed areas the ground surface varies between 0.5 and 4 m a.s.l. These ridges comprise high permeability gravelly materials with sandy loam matrix (Fig. 1) and marked calcium carbonate cementation covered by wind deposited sandy sediments (Carol et al., 2024). The cementation of the sediments reduces the recharge of rainwater through infiltration and leads to the accumulation of soluble salts on the surface. This conditions the groundwater chemistry, which tends to be sodium chloride and brackish in certain areas (Carol et al., 2021). Despite this limitation caused by salinity, the water is still used by the rural population for livestock activities.

Holocene ridges are constituted by N-S oriented deposits as well, that diffracted toward the N-W direction in the north sector due to coastal drift as the beach ridge plain developed. These deposits reach elevations of almost 8 m a.s.l. in the central sector decreasing towards the edges. Geological formations characteristics within this area are quite heterogeneous with predominantly high permeability lithologies made of gravel and sandy matrix. These beach ridges store freshwater of the sodium-calcium bicarbonate type (Carol et al., 2021), which is used to supply the coastal population.

2.2. Climatic indicators and time-series analysis

Precipitation and temperature for the study area were retrieved from E. E. A. Hilario Ascasubi meteorology station (39°23′S, 62°37′W) of the Instituto Nacional de Tecnología Agropecuaria (INTA, 2024) and analysed for the period 1967–2022, while soil moisture storage capacity was calculated taking into consideration both the soil texture and present vegetation defined for the soils found in the study area (INTA et al., 2024b). To assess hydrological wet or dry conditions the Standardized Precipitation Evapotranspiration Index (SPEI) was utilized, integrating both precipitation and potential evapotranspiration in its formula (Vicente-Serrano et al., 2010). The SPEI Global Drought Monitor was questioned to obtain the data, available on the official SPEI website (SPEI Global Drought Monitor (csic.es)) (Vicente-Serrano and Beguería, 2016). Data were downloaded for the same period (1967–2022), at the large scale of 12 months relevant for climate-driven impacts, and with a spatial resolution of 0.5°. The index values range from ≥2 (extremely wet) to ≤ −2 (extremely dry), being near normal conditions the values within the range of 0.99 to −0.99 (Table 1) (Li et al., 2015). This index has been found useful to analyze groundwater table variations around the world (Bohn et al., 2020; Secci et al., 2021; Shayeghi et al., 2024).

Table 1
Classification of categories according to SPEI values (Taken from Li et al., 2015).

SPEI	CATEGORIES
≥2	Extremely wet
1,5 to 1,99	Very wet
1 to 1,49	Moderately wet
−0,99 to 0,99	Near normal
−1 to −1,49	Moderately dry
−1,5 to −1,99	Very dry
≤ −2	Extremely dry

Likewise, ENSO events were classified into El Niño (EN), La Niña (LN) and neutral phase according to the Oceanic Niño Index (ONI), developed by the National Oceanic and Atmospheric Administration (NOAA). This index is defined as the three-month running mean of Equatorial Pacific Ocean Sea surface temperature (SST) anomalies in the Niño 3.4 region (5°N-5°S y 120-170°W) that exceed the ±0.5 °C threshold. The index must exceed the threshold for at least five consecutive overlapping seasons. EN events are those in which the temperature anomalies recorded are positive, while LN is characterized

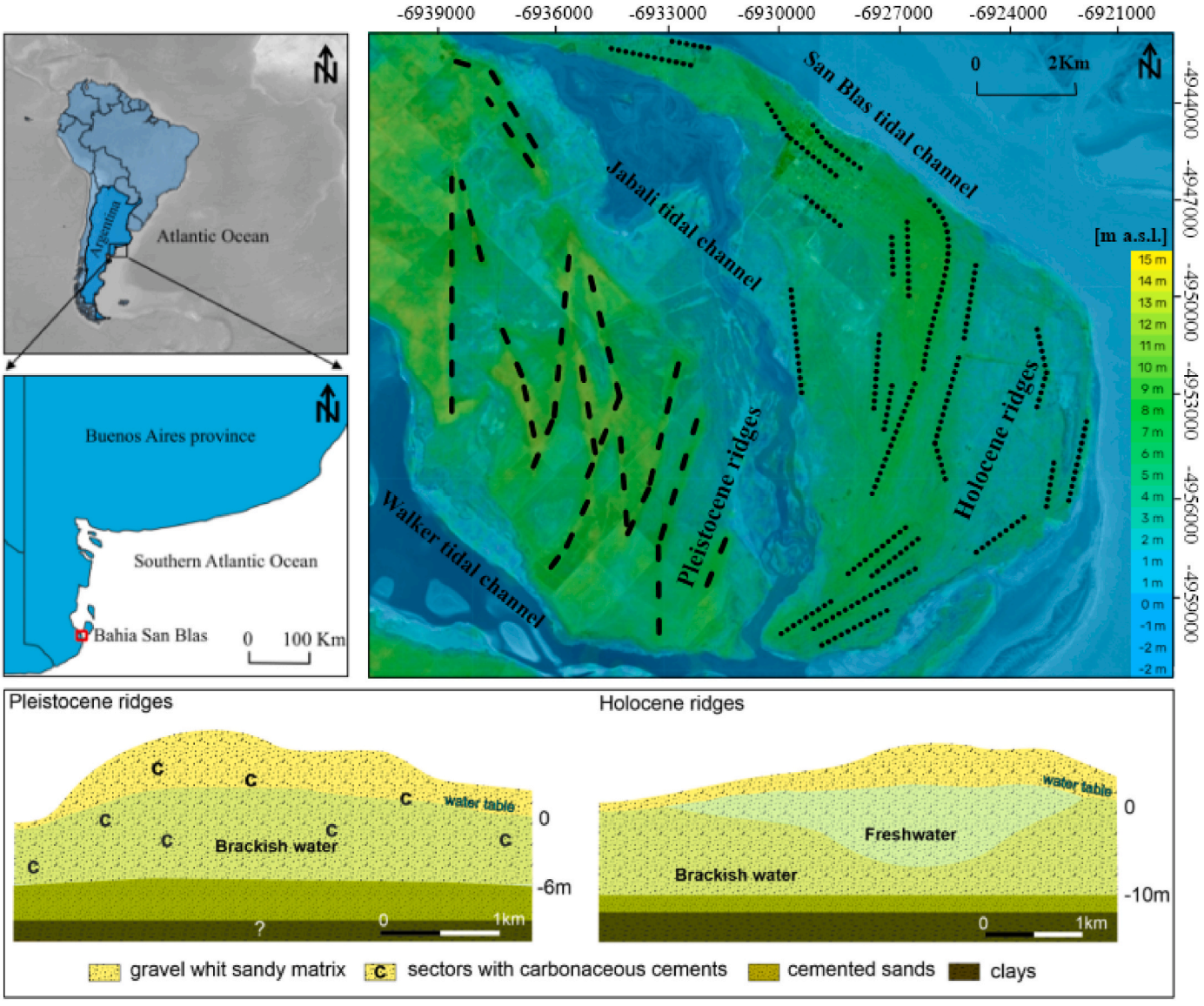

Fig. 1. Location of the study area with topographic map indicating Pleistocene (dashed lines) and Holocene littoral ridges (dotted lines) and corresponding hydrogeological cross-sections.

by negative anomalies, belonging to a neutral phase those years in which there are no anomalies, or the threshold of five consecutive overlapping seasons is not exceeded. ONI index data for the years 1967–2022 were obtained from NOAA website (https://www.cpc.ncep.noaa.gov/data/indices/oni.ascii.txt.)

For the water balance calculation, the online app WaterbalANce (Mammoliti et al., 2021) was utilized. This app, based on the Thornthwaite–Mather method (https://thornwaterbalance.com/), requires the following input parameters: the latitude of the study area (LAT, decimal degrees), the mean monthly temperature (Tm, degrees Celsius), the monthly total precipitation (P, millimeters) and the soil moisture storage capacity (SM, millimeters).

To assess the associations between variables of different types, a comprehensive statistical approach was followed computing Pearson (P) (i.e. parametric test for linear correlation), Kendall (K), and Spearman (S) (i.e. non-parametric tests for statistical dependence) correlation coefficients. The analysis, performed in IBM-SPSS 30.0 environment, allowed to measure the strength and direction of association between the variables. Values of ±1 indicate a perfect association, while values closer to zero indicate weaker relationship. The sign of the coefficient indicates a positive and negative relationship (Chen and Popovich, 2002). Cohen et al. (2003) standard was used to determine the effect size of the relationship: correlation coefficients between 0.10 and 0.29 represent a small association, between 0.30 and 0.49 a medium association, and coefficients above 0.50 represent a large association. In all the analysis, *P*-values <0.05 were considered as statistically significant.

Furthermore, a contingency analysis on seasonal climatic data was performed to examine the relationship between ONI and SPEI categories. This method is better suited in examining whether two climatic phenomena are linked in any way by focusing on the co-occurrence of events, rather than correlation analysis which may fail in cases of extreme events (Davey et al., 2014).

2.3. Numerical model set up

All the available hydrogeological and stratigraphic information were integrated to develop a 3D GW flow model able to estimate GW table oscillation over the study period and assess the GW flow budget at the aquifer scale. Data were elaborated in GIS environment and processed via Processing Modflow 11 graphical user interface (Chiang, 2022). The flow simulation was carried out using the MODFLOW-NWT code (Niswonger et al., 2011), describing the three-dimensional movement of GW through a porous matrix with the partial differential equation:

$$\frac{\partial}{\partial x}\left[K_{xx}\frac{\partial h}{\partial x}\right]+\frac{\partial}{\partial y}\left[K_{yy}\frac{\partial h}{\partial y}\right]+\frac{\partial}{\partial z}\left[K_{zz}\frac{\partial h}{\partial z}\right]+W=S_s\frac{\partial h}{\partial t} \quad (1)$$

where K_{xx}, K_{yy} and K_{zz} are values of hydraulic conductivity along x, y and z coordinate axes (LT^{-1}); h is the potentiometric head (L); W is a volumetric flux per unit volume representing sources and/or sinks of water (T^{-1}); Ss is the specific storage of the porous media (L^{-1}); and t is time (T).

The model domain was discretized into a regular spaced grid of 165 m × 165 m that consisted of 100 rows, 100 columns and 4 layers with variable thickness.

A Digital Elevation Model from Instituto Geográfico Nacional (IGN, 2024) (https://www.ign.gob.ar/NuestrasActividades/Geodesia/ModeloDigitalElevaciones/Introduccion) with a spatial resolution of 30 × 30 m cells was employed to acquire topographic information and represent morphology. The top of the grid was interpolated, ranging from −8 m to 21 m a.s.l. Vegetation, buildings, and other anthropic features were removed digitally to ensure accuracy, resulting in a refined terrain model. Hydraulic conductivity values from pumping tests (for gravelly strata) and constant head lab tests (for sandy loams) were averaged and imported via polygons input method to get a representative value for each geological formation in the study area. The horizontal hydraulic conductivity values range from $1x10^{-6}$ m/s where sandy loam layers are present, to $1x10^{-3}$ m/s in gravelly strata.

Atlantic Ocean levels were retrieved from the Copernicus Marine Service (CMEMS) (https://doi.org/10.48670/moi-00021) covering a 29 years period (from 1993 to 2022). An averaged value (0.13 m) was set and incorporated within the MODFLOW's Constant Head Boundary Package (CHB), accounting for the seawater (SW) systems (Atlantic Ocean and tidal channels in Fig. 1) as model boundary conditions. Groundwater head values from 4 to 6.35 m a.s.l. were imported via polyline input method within the same CHB package, to mimic the regional inflow from the inland western part of the Pleistocene ridges (Regional CHB in Fig. 2).

WaterbalANce derived recharge and evapotranspiration rate data were used as input boundary conditions to inform the hydrogeological model. QGIS 3.36 software (http://www.qgis.org) was used to process the data by trimming the files, change coordinates and format to simulate them within the Recharge and Evapotranspiration Package (RCH and EVT), respectively.

At first, a steady-state simulation was run under average condition and the model was calibrated via trial-and-error technique against observed piezometric heads recorded for the year 2021 (Fig. 2). Groundwater monitoring points correspond to pre-existing boreholes (domestic supply wells or mills). In the Holocene ridges, the boreholes are drilled to an average depth of 6 m, with a 1-m filter at the base, and take water from the shallowest freshwater section of the aquifer housed in gravels with a sandy matrix. In the Pleistocene ridges, the boreholes are drilled to a depth of 5–7 m, drawing water from the aquifer housed in the partly cemented gravels above the cemented sands (Fig. 1). Observed heads at each monitoring well (white cross in Fig. 2) were compared to simulated values at corresponding locations and physically based hydraulic conductivity values were adjusted to optimize model performances. The coefficient of determination (R^2), the Nash–Sutcliffe model efficiency coefficient (NSE), and the mean squared error (MSE) were used to evaluate model accuracy.

A sensitivity analysis was performed using single perturbation tests (±10% of the employed parameter values) on the calibrated model recharge rates, evapotranspiration rates and extinction depths. The analysis ensured the resilience of the model's performance to small changes in key input parameters.

Then, the calibrated piezometry was imported as initial condition for a fully transient simulation over 56 yearly stress periods (1967–2022) each one divided into 4-time steps of seasonal length. This approach allows to infer changes in GW heads and flows due to varying recharge and evapotranspiration rates, elucidating the interplay among climate patterns and subsurface systems.

To support the simulation results, the open-source web application called GRACE Groundwater Subsetting Tool (GGST) (McStraw et al., 2022) was interrogated to retrieve the GW storage (GWS) within the Bahia San Blas coastal aquifer (https://apps.geoglows.org/apps/ggst/global-map/). GRACE data, provided at monthly intervals in equivalent water thickness (in centimeters) with a spatial resolution of 1°, were converted in m^3/s over a 20-year period (from April 2002 through February 2022) according to the model's unit and compared with the calculated net storage. GRACE satellites provided an independent dataset for GWS that was used to validate the transient numerical model.

Finally, the same statistical approach described in section 2.2 was applied to estimate the relationship between climatic drivers, simulated budget components and GW level fluctuations over time.

The research workflow is represented in Fig. 3.

3. Results

3.1. Precipitation and climate variability

To identify relationships among meteoric forcing, hydrogeological patterns and climatic cycles at the aquifer scale, multiple time-series

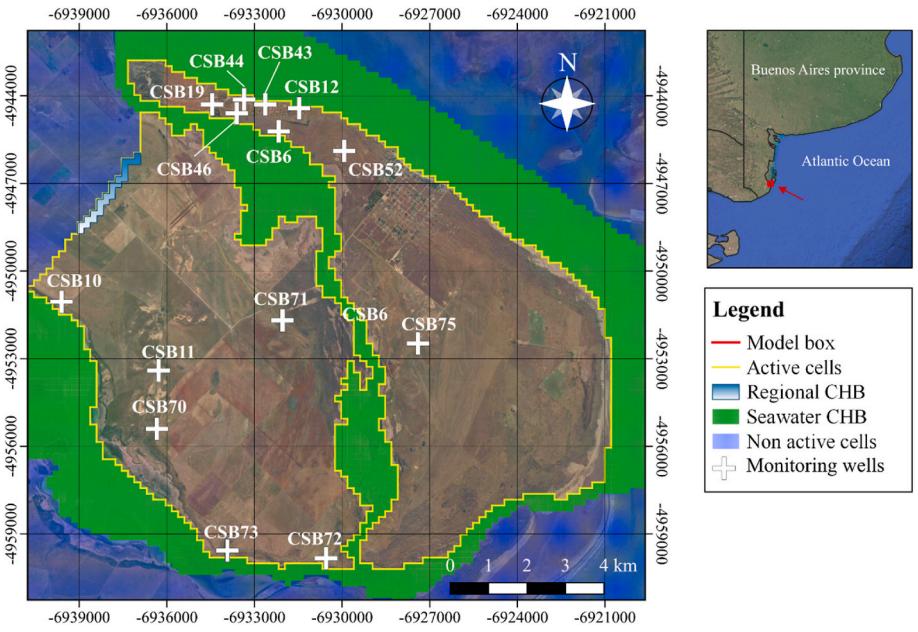

Fig. 2. 2D representation of the simulated area and the boundary conditions used to constrain the model.

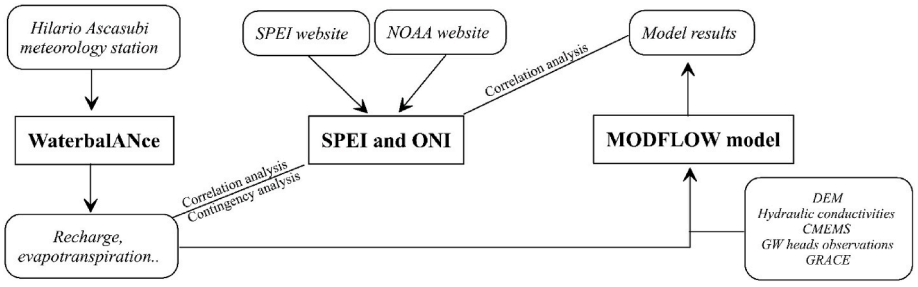

Fig. 3. Chart of the research workflow.

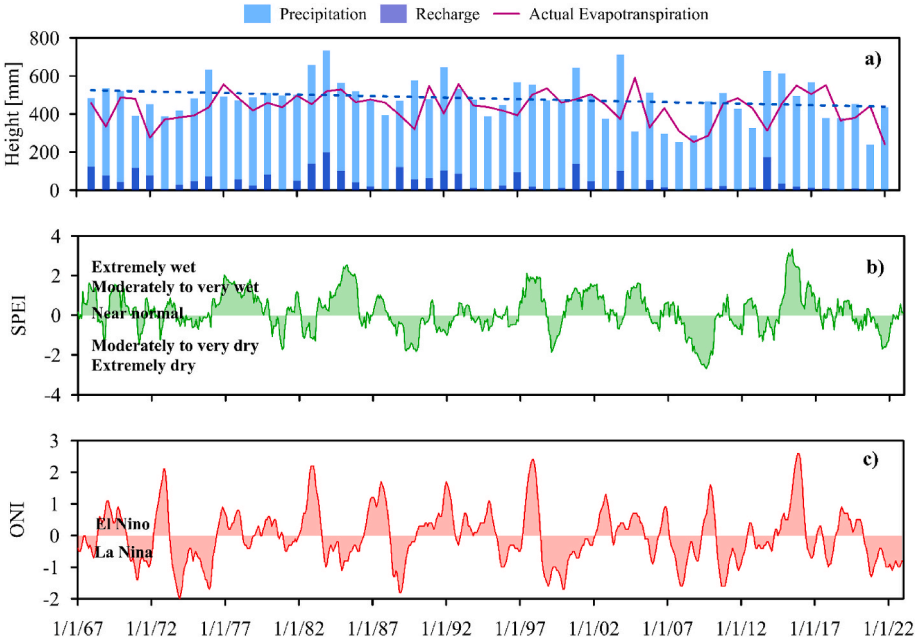

Fig. 4. Cumulated annual precipitation (with linear trend, dashed line) and WaterbalANnce-derived aquifer recharge and actual evapotranspiration **(a)** together with SPEI **(b)** and ONI index **(c)** over the study period 1967–2022.

datasets, including i) annual cumulative precipitation values from meteorological station, ii) WaterbalANce-derived GW recharge and evapotranspiration, iii) categorized SPEI and iv) ONI values, were plotted together in Fig. 4.

The analysis of precipitation data reveals a slight declining trend within the observed period, with an average annual precipitation value of 485 mm, reaching a maximum of 733 mm in 1984 and a minimum of 238 mm in 2021 (Fig. 4a). WaterbalANced-derived GW recharge follows the precipitation trend, with a mean value of 49 mm, accounting for 10% of total precipitation income. It reaches its maximum in the same year (1984), while many years exhibit negligible or no recharge. Conversely, the actual evapotranspiration, calculated using the same approach, presents a quite stable trend within the observed period with an average value of 430 mm (Fig. 4a).

The SPEI analysis allows the recognition of normal, dry and wet events within the study period (Fig. 4b). Numerous moderately wet to very wet events (SPEI between 1 and 2) are identified, while few extremely dry events occurred (1984 and 2015–2016). Moderately dry to very dry events (SPEI between −1 and −2) are also numerous, but in smaller proportion than the wet ones.

Only few extremely dry event (SPEI < −2) (2008–2009) were recorded during the analysed time. Near normal conditions (SPEI between 1 and -1) are distributed throughout the entire period, alternating with both wet and dry episodes.

The ONI analysis provides insight into the alternation of EN and LN events of varying intensity between 1967 and 2022 (Fig. 4c). Generally, EN events (positive ONI values) tend to coincide with periods of higher mean annual precipitation and wet conditions as recognized by the SPEI, with some exceptions (e.g., 1985). Conversely, LN (negative ONI values) are more frequently associated with medium to low values of mean annual precipitation and dry periods.

To quantify these potential associations a statistical analysis was performed, and Pearson (P), Kendall (K), and Spearman (S) coefficients computed assessing the numerical correlation among all datasets in Fig. 4.

Table 2 indicates a positive correlation between ENSO-related events, SPEI variations and mean annual precipitation. A small to medium association was found between the datasets with coefficient ranging from 0.18 to 0.34. This confirms how alternating EN and LN 'ENSO' phases are non-negligible in affecting wet and dry periods conditions.

Likewise, actual evapotranspiration exhibits a small to medium association with ONI and correlation coefficients values range from 0.21 to 0.33. On the contrary, calculated aquifer recharge shows no significant correlation with either ONI or SPEI, as the significance value exceeded the 5% threshold. This suggests that any linear relationship detected is probably random and not indicative of a real pattern.

A medium to large association was observed between SPEI and precipitation (coefficient from 0.33 to 0.53). A slightly larger association was detected between SPEI and evapotranspiration with coefficients from 0.37 to 0.58.

Recharge and evapotranspiration resulted to be largely correlated with the precipitation with correlation coefficients ranging from 0.53 to 0.87, while no linear relationship was found between them (P value non-significant). They are likely monotonically related, and the relationship may involve non-proportional changes (S = 0.79).

When dealing with relationships between discrete climatic events, correlation analysis may fail in cases of extremes that can bias the results making it less reliable for detecting meaningful patterns. Conversely, contingency analysis offers more relevant insights for risk assessment and management than statistics (Davey et al., 2014). The method is also easier to explain and doesn't require specialist climatic or statistical expertise. The approach consists of calculation of contingency tables based into three 'ONI' categories: i) El Nino (EN), ii) La Nina (LN), and iii) neutral phase; and seven target SPEI categories (Table 1).

As illustrated by the cluster bar chart in Fig. 5, EN 'ONI' category is clearly associated with a higher frequency of wet periods as identified by the SPEI. Particularly, the rate of occurrence of extremely wet events within the EN 'ONI' category increases by 7.4 % compared to Neutral 'ONI' category (7.8 against 0.4%). Near normal periods and dry events significantly decrease, except for extremely dry events rate of occurrence that slightly increases.

Conversely, LN 'ONI' category correlates more with dry periods with a slight increase in very dry to extremely dry events compared to neutral phase. Near normal events rate of occurrence identified by the SPEI also slightly increases within the LN 'ENSO' phase.

Overall, EN 'ONI' category seems to exert a most pronounced influence on SPEI categories distribution during the observed period.

It is important to keep in mind that, even if historical rates of occurrence provide general guidance for water resource management, each ENSO event is individual and occurs in combination with other climatic factors (Davey et al., 2014). Because of the complex interconnection among climatic factors, this analysis should not be considered as a strictly predictive tool for imminent or ongoing ENSO events.

3.2. Model outputs and climatic impact on calculated results

GW levels for the year 2021 from all the monitoring wells displayed in Fig. 2 were used to verify the ability of the model to reproduce the piezometric conditions in the coastal aquifers. The model effectively captures the magnitude and areal variability of GW levels within the study area, achieving excellent model performance indicators (R^2 = 0.982, NSE = 0.977 and MSE = 0.026 m^2).

It must be stressed that calculated levels in the model cells

Table 2
Correlation analysis matrix between climatic indicators and main hydrological budget components.

		ONI	SPEI	Precipitation	Recharge	Evapotranspiration
ONI	P	1	0.31	0.3	*0.13*	0.33
	K	1	0.18	0.21	*0.17*	0.21
	S	1	0.28	0.34	*0.25*	0.31
SPEI	P		1	0.53	*0.23*	0.58
	K		1	0.33	*0.17*	0.37
	S		1	0.48	*0.25*	0.54
Precipitation	P			1	0.69	0.87
	K			1	0.53	0.7
	S			1	0.71	0.59
Recharge	P				1	*0.26*
	K				1	0.24
	S				1	0.79
Evapotranspiration	P					1
	K					1
	S					1

*Correlation coefficients in *italic* represent a non-significant correlation (p-value >0.05).

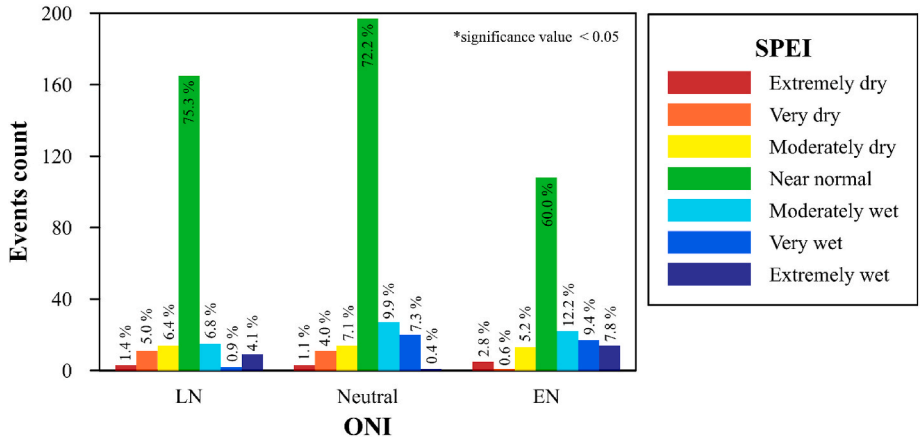

Fig. 5. Cluster bar chart displaying results (events count and rates of occurrence in percentage of categorized SPEI values within ENSO climatic oscillation) of contingency analysis.

corresponding to the monitored piezometers do not account for local factors that couldn't be accurately monitored and considered within the simulation (e.g. uncontrolled and non-monitored GW extraction).

A single parameter sensitivity analysis was performed to elucidate the uncertainties in recharge rates and evapotranspiration rates and extinction depth (right panels in Fig. 6). The results highlighted a weak overall sensitivity to ±10% parameter perturbations, with minor differences on all the model performance indicators: the recharge rate perturbation induced model performance changes of ≈0.01, 0.02 and 0.03 m^2 on the R^2, NSE and MSE, respectively; the evapotranspiration rate and extinction depth perturbations induced even smaller changes of ≈0.01 for both the R^2 and NSE and between 0.01 and 0.02 m^2 on the MSE.

The transient simulation provided a GW fluctuations estimate throughout the simulation, revealing significant water table variations over space and time due to surface topography and climate cycles, respectively. The water table is in general high in areas of higher elevation and decrease in low-lying discharge zones. Flow lines are radially oriented toward the Atlantic Ocean and tidal channels, locally influenced by spatial variations in hydraulic conductivity.

Moreover, the fluctuating meteoric recharge associated to variable climatic conditions significantly influenced GW dynamics over the study period. Fig. 7 shows a comparison between GW heads maps from two different periods of the simulation: i) 1984, a wet period characterized by high meteoric recharge associated to EN 'ENSO' phase (Fig. 7a) and ii) 2022, a dry period with minimal meteoric recharge associated to the last LN 'ENSO' phase (Fig. 7b). The comparison underlines a clear decline in GW heads across the study area, with an average drop of approximately 2 m, documenting how wet and dry periods associated with different climatic phases influence the aquifer system.

To gain a deeper understanding of the GW head dynamics, the Processing Modflow Zone Budget routine (Harbaugh, 2005) was run and the volumetric water budget within the model domain assessed, accounting for recharge and evapotranspiration patterns, together with SW-GW water volume exchange (Fig. 8). To focus on SW-GW water volume exchange, user-defined zones within the model domain were defined by

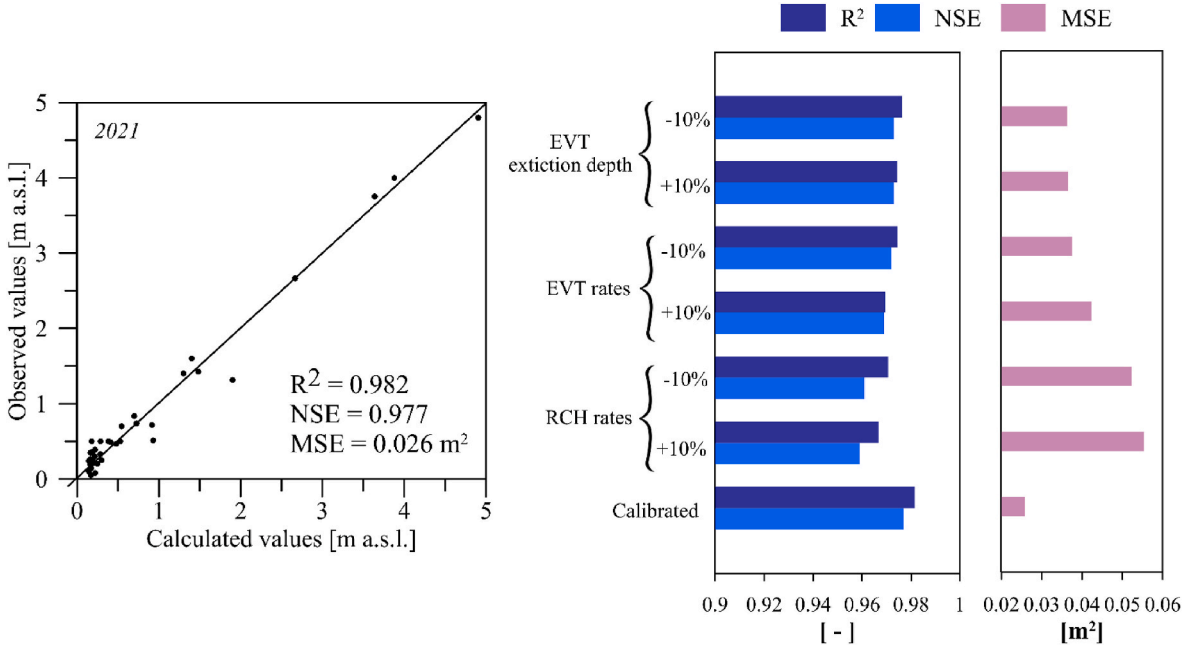

Fig. 6. Head scatter diagram representing calculated versus observed piezometric heads for the year 2021 and the model performance indicators (left panel); sensitivity analysis on the main hydrogeological budget component demonstrating the impact of the single perturbation test on the model performance indicators (right panels).

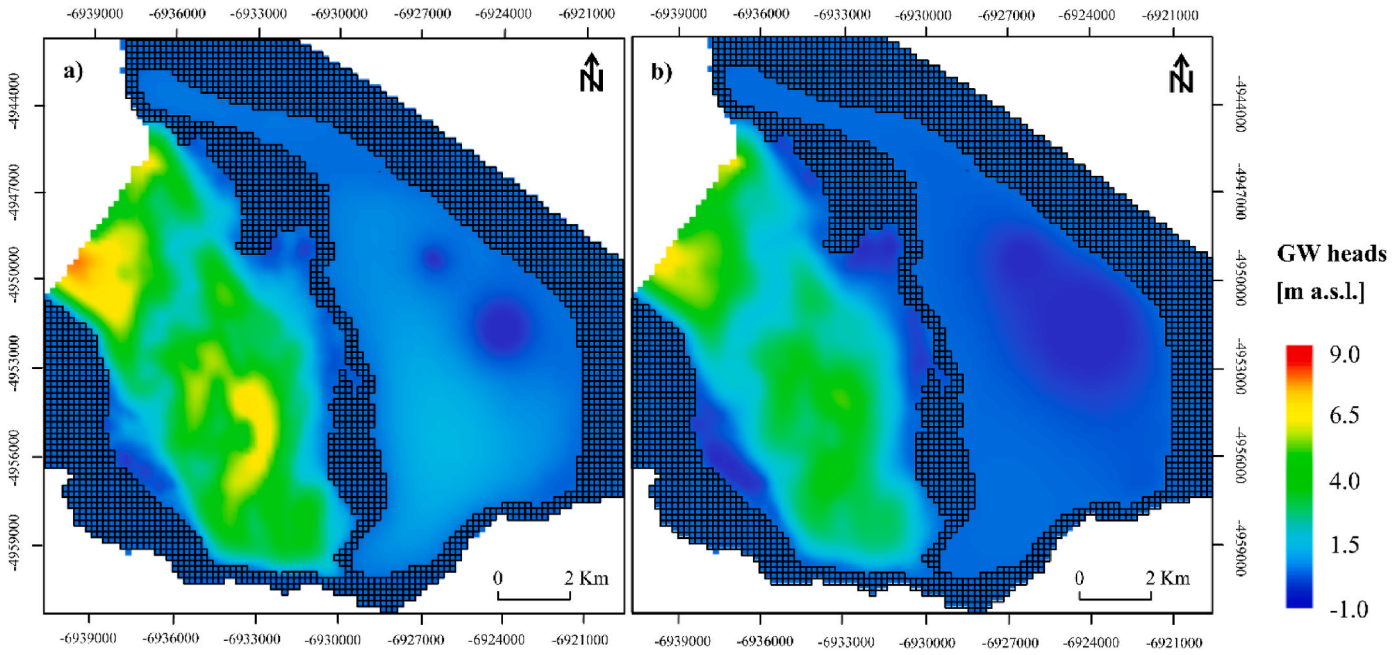

Fig. 7. Maps of calculated GW heads during **a)** wet period associated with high meteoric recharge (1984) and **b)** dry period associated with low meteoric recharge (2022).

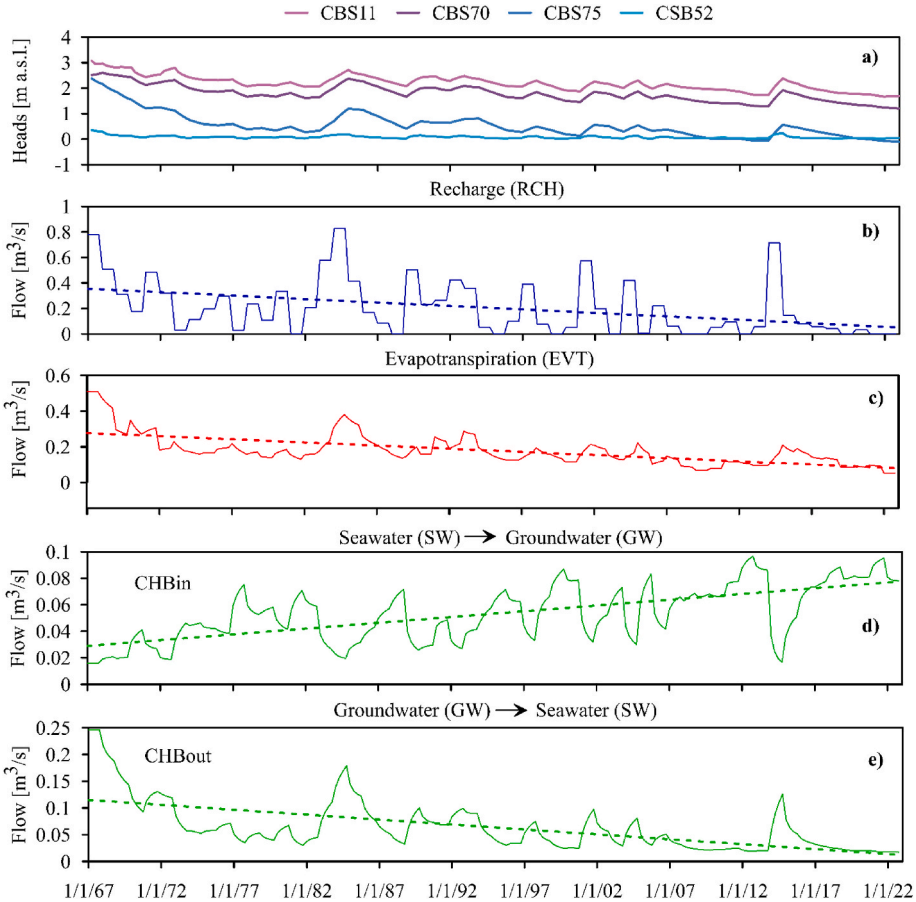

Fig. 8. Calculated GW heads in selected observation points (**a**), calculated recharge (**b**), calculated evapotranspiration (**c**) and calculated SW-GW exchange (**d** and **e**) over the simulated period (1967–2022).

assigning zone numbers to model cells, accounting for regional and seawater inflow components separately.

Calculated GW levels oscillated according to recharge and evapotranspiration patterns presenting peaks and troughs during wet and dry periods (Fig. 8a). Clear declining trends were observed over the simulation time at each monitoring well mimicking the decline observed in recharge rate over the study period.

Recharge and evapotranspiration emerged as the major inflow and outflow to/from the aquifer system, both varying throughout the simulation according to changes in precipitation. High recharge rates values were observed during wet seasons, reaching maximum flow rate of almost 0.83 m^3/s in the year 1984 in correspondence of the wettest year (precipitation >700 mm). Negligible or no meteoric recharge was observed during other years within the simulation time (e.g. year 1981, 1988, 1995, 1999, 2003, 2008, 2009, 2012, 2019, 2021 and 2022).

Fig. 8c is showing that the evapotranspiration from GW is also declining over the simulation time. This trend is likely due to the lowering of water table which reduces the volume of water available for direct evaporation pushing the water table below the evapotranspiration extinction depth threshold (Colombani et al., 2021).

The water flow exchange between SW and GW systems varies significantly throughout the simulation (Fig. 8d and e). At the beginning of the simulation, the aquifer predominantly discharged toward SW bodies (Atlantic Ocean and tidal channels) with a flowrate approximately ten times higher than the flowrate from these SW bodies (0.25 against 0.02 m^3/s, respectively). However, the progressive depletion of GW resources due to reduced meteoric recharge altered the equilibrium within the systems, with a clear increase in SW flow contribution toward the GW system. Because of this, at the end of the simulation the GW discharge toward the SW bodies was four times lower than the inflow received from them (0.02 against 0.08 m^3/s, respectively). Considering Southern Atlantic Ocean salinity values of about 36 g/L, this CC-driven shift in water exchange dynamics could even alter the salinization dynamics settled among SW and GW systems, potentially exacerbating SW intrusion and consequently worsening GW quality in low-lying regions. Considering that the population of Bahía San Blas has increased considerably in recent years, it is to be expected that there will be greater demands for water supply. Consequently, the increased exploitation of the aquifer would further aggravate the situation in the future.

4. Discussion

Concerns regarding CC impacts, together with overexploitation and depletion of many aquifers worldwide, are leading to a growing interest in globally assessing GWS changes (Kamali and Asghari, 2023; Feng et al., 2017). Satellite gravity measurements from the Gravity Recovery and Climate Experiment (GRACE) offer a unique tool that could be used as an independent dataset for monitoring GWS changes on a global scale in absence of continuous GW monitoring network.

GWS calculated by the model and from GRACE were compared over 20 years (2002–2022). Although the current GRACE product is limited by its coarse resolution, it remains useful for understanding the magnitude and temporal variability of water storage of individual aquifers (Sun et al., 2012). The comparison illustrated in Fig. 9 shows how the model and remote sensing dataset are within the same order of magnitude. However, some discrepancies in their respective trends and values are evident. GRACE data indicates a declining GWS trends, while the numerical model suggests a more stable trend and generally higher GWS values. This divergence among the two derived GWS is consistent with insights from other studies that tried to compare models results with satellite-derived data. As an example, Rateb et al. (2020) tried to compare GWS from GRACE and from regional models in 14 major U.S. aquifers highlighting how models generally show similar or greater GWS trends than those from GRACE.

Moreover, the coarse resolution of GRACE could result in the inclusion of additional discharge zones, leading to an underestimation of GWS compared to the model-derived values. This is particularly relevant in coastal aquifers where localized processes may not be fully captured by GRACE. Conversely, the model may provide a more refined representation of GWS dynamics within the study area by incorporating smaller-scale hydrogeological features. Downscaling the remote sensing dataset at a sub-GRACE-resolution scale to address this limitation could be useful from a management perspective, since water managers rely on models to examine GWS changes at areas smaller than GRACE resolution (Lo et al., 2010; Sun et al., 2012).

The multiscale approach used, integrating large scales climatic indices and numerically calculated hydrological datasets, provided valuable insights in the relationships between climate patterns, meteorological variability and the local scale coastal aquifer. Such an approach, even if it may result in some discrepancies between the datasets due to differences in spatial and temporal resolution, aligns with prior studies that focus on assessing the impact of climatic stressors on local or regional hydrologic systems (Rasouli et al., 2020; Archer and Fowler, 2004; Balacco et al., 2022).

The impact of climatic stressors and the calculated water budget components on GW levels time-series, calculated at each monitoring well, was assessed via statistical analysis, computing P, S and K correlation coefficients (Table 3).

Results indicate that EN and LN 'ENSO' phases have a minimal impact on GW oscillation within the study period. No significant linear association were identified through parametric statistical analysis (P values have no statistical significance), while the non-parametric measurements revealed a small monotonic association between ONI and calculated GW level fluctuations recorded at most observation points (K and S range from 0.19 to 0.3).

Similarly, a small positive, mostly non-linear and monotonic correlation was found between SPEI values and GW levels, with coefficient reaching a maximum of 0.32. This insight indicates a minor but noticeable relationship between wet and dry periods interchange and the GW system.

The statistical analysis confirmed the huge contribution of both calculated recharge and evapotranspiration in shaping the GW budget: a

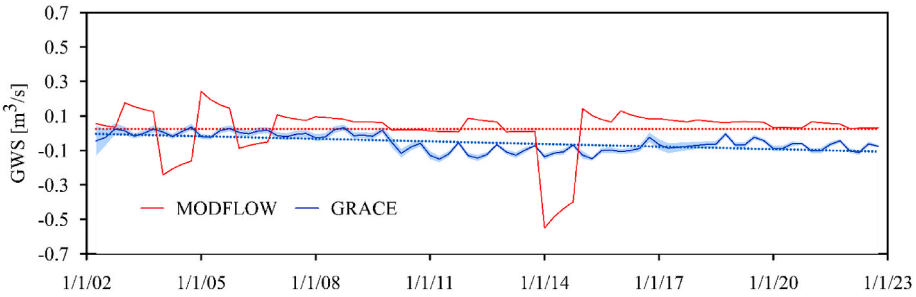

Fig. 9. Comparison between the simulated net storage (red line) and the GRACE remotely sensed groundwater storage (blue line) with its low and high error range (shaded blue band); linear trends of both the time-series were represented with dashed lines.

Table 3
Impact of climatic indicators and calculated budget components on GW level fluctuations.

		CSB 6	CSB10	CSB11	CSB12	CSB19	CSB43	CSB44	CSB46	CSB52	CSB70	CSB71	CSB72	CSB73	CSB75
ONI	P	*0.17*	*0.15*	*0.16*	*0.18*	*0.18*	*0.18*	*0.17*	*0.17*	*0.21*	*0.17*	*0.20*	*0.20*	*0.21*	*0.14*
	K	*0.16*	*0.14*	*0.18*	0.20	0.20	0.20	0.20	0.20	0.19	0.19	0.20	0.21	0.20	*0.17*
	S	*0.24*	*0.19*	*0.23*	0.29	0.30	0.30	0.30	0.30	0.28	*0.25*	0.27	0.29	0.27	*0.22*
SPEI	P	*0.22*	*0.23*	*0.22*	0.28	0.29	0.29	0.29	0.29	*0.24*	*0.25*	0.28	0.30	*0.26*	*0.23*
	K	*0.13*	*0.15*	*0.16*	0.20	0.22	0.21	0.22	0.22	*0.16*	0.19	0.20	0.20	*0.17*	*0.17*
	S	0.20	0.20	0.22	0.30	0.32	0.30	0.32	0.32	0.24	0.25	0.27	0.28	0.24	0.22
[a]**RCH**	P	0.97	0.61	0.61	0.98	0.98	0.98	0.99	0.99	0.95	0.61	0.63	0.67	0.70	0.56
	K	0.81	0.46	0.50	0.85	0.88	0.87	0.88	0.88	0.78	0.47	0.48	0.53	0.55	0.43
	S	0.94	0.64	0.69	0.97	0.98	0.97	0.98	0.98	0.93	0.66	0.66	0.66	0.72	0.74
[b]**EVT**	P	0.77	0.90	0.87	0.84	0.84	0.84	0.84	0.84	0.79	0.90	0.91	0.93	0.91	0.89
	K	0.53	0.71	0.71	0.65	0.69	0.67	0.68	0.68	0.57	0.73	0.75	0.79	0.73	0.70
	S	0.74	0.89	0.88	0.84	0.86	0.85	0.86	0.86	0.78	0.90	0.91	0.93	0.9	0.88
[c]**CHB in**	P	−0.91	−0.77	−0.79	−0.89	−0.87	−0.88	−0.87	−0.87	−0.92	−0.78	−0.79	−0.8	−0.85	−0.73
	K	−0.82	−0.61	−0.68	−0.78	−0.73	−0.76	−0.74	−0.74	−0.86	−0.63	−0.62	−0.66	−0.72	−0.58
	S	−0.95	−0.79	−0.86	−0.94	−0.91	−0.93	−0.91	−0.91	−0.97	−0.82	−0.81	−0.85	−0.90	−0.77
[d]**CHB out**	P	0.93	0.86	0.87	0.95	0.94	0.95	0.94	0.94	0.94	0.87	0.87	0.91	0.91	0.85
	K	0.72	0.72	0.75	0.80	0.81	0.81	0.81	0.81	0.77	0.74	0.74	0.79	0.79	0.70
	S	0.89	0.87	0.90	0.95	0.95	0.95	0.95	0.95	0.92	0.89	0.89	0.93	0.94	0.85
GWS in	P	−0.48	*0.13*	*0.11*	−0.45	−0.47	−0.45	−0.46	−0.46	−0.41	*0.13*	*0.12*	*0.08*	*0.02*	*0.18*
	K	−0.45	*0.02*	*−0.02*	−0.39	−0.38	−0.39	−0.39	−0.39	−0.39	*0.02*	*0.01*	*−0.02*	*−0.07*	*0.05*
	S	−0.62	*0*	*−0.07*	−0.55	−0.55	−0.55	−0.55	−0.55	−0.55	*−0.01*	*0*	*−0.08*	*−0.13*	*0.05*
GWS out	P	0.65	*0.04*	*0.05*	0.62	0.63	0.62	0.63	0.63	0.60	*0.04*	*0.06*	*0.11*	*0.16*	*−0.01*
	K	0.52	*0.05*	*0.09*	0.45	0.44	0.45	0.45	0.45	0.47	*0.06*	*0.05*	*0.09*	*0.14*	*0.01*
	S	0.70	*0.11*	*0.17*	0.6	0.59	0.60	0.60	0.60	0.63	*0.12*	*0.11*	*0.18*	*0.23*	*0.05*

*Correlation coefficients in *italic* represent a non-significant correlation (p-value >0.05).
[a] RCH: calculated recharge.
[b] EVT: evapotranspiration.
[c] CHB in: seawater flows toward the aquifer (SW→GW).
[d] CHB out: aquifer discharge toward the ocean and tidal channels (GW→SW).

large association between GW oscillation and calculated recharge and evapotranspiration was detected with correlation coefficient ranging from 0.43 to 0.99.

The relationship between SW and GW systems was also investigated. Correlation coefficients between SW flow into the aquifer (CHB in) and GW levels range from −0.58 to −0.97 representing a large negative association among the two datasets. This suggests that as the GW levels rise, less water flows into the aquifer from the Ocean and tidal channels, and conversely, higher SW inflows are associated with lower GW levels. Consequently, a large positive association was detected between GW levels and GW discharge towards SW systems (CHB out) with coefficients ranging from 0.70 to 0.95.

The analysis of GWS changes revealed a varying association across the study area. Calculated GWS seems to be mostly associated (from medium to large effect size) with GW levels within the Holocene coastal area of the model domain, while no statistically significant associations were detected with GW levels recorded within the Pleistocene area (e.g. CSB10, CSB11, CSB70, CSB71, CSB72, CSB73). This is probably due to the superficial cementation associated with lower hydraulic conductivity values and higher residence times, that make GW levels fluctuations less sensitive to GWS changes. Overall, this study identified valuable patterns quantifying the relationship between climatic cycles, meteoric forcing and hydrogeological features calculated at the aquifer scale. While the associations between GW levels fluctuations and both ENSO and SPEI values are of small effect size, they offer useful information for prospecting changes in freshwater resources availability in similar areas along the arid Patagonian coast where populations are experiencing serious freshwater supply challenges.

Linking hydrogeological variability within a local or regional basin to global climate patterns can be used to further develop land-atmosphere interactions that consequently provide an opportunity to better manage water resources in the future (Rasouli et al., 2020). In the last decades, researchers have been relying on remote sensed databases that are providing the community with a growing quality of climate and hydrogeological datasets, in terms of coverage, spatial and temporal resolution. However, the use of multi scalar datasets to estimate the climate variability impact on small basins brings with it many uncertainties. First, most of these datasets are still too coarse to properly reproduce local conditions. Second, many of the recommendations outlined, like dataset downscaling and other tailoring methods, have great time and computational costs (Holman et al., 2012). Considering all the limitations related to the multiscale approach used, it must be stressed that the analysis of the aquifer response to multivariate processes (e.g. changing climatic conditions) should be assessed in a particularly careful way, and the correlations should not be interpreted as indicative of a teleconnection relationship among climate and GW systems without further analysis.

5. Conclusions

In this study, climatic indices and hydrological datasets were integrated to assess the complex interplay between environmental changes related to climate cycles and GW system dynamics over a long-term period (1967–2022).

The analysis of the SPEI and ONI allows for the recognition of normal, dry and wet events associated to varying ENSO phases within the observation period. The statistical correlation and contingency analysis provide valuable insights, showing a limited but noticeable association between ONI, SPEI and mean precipitation values. EN phase of ENSO results to induce the most evident effect on SPEI categories distribution, with an increasing rate of occurrence of moderately to extremely wet events compared to Neutral phase.

The numerical simulation allowed for the assessment of temporal and spatial evolution of GW fluxes within the coastal aquifer, allowing an accurate hydrogeological balance calculation. Very good calibration was accomplished with high model performance indicators (sensitivity analysis confirmed the model robustness as perturbations of key parameters had a minor influence on performance). The model successfully captured GRACE-derived GWS order of magnitude but underscoring some limitations within this remote sensed dataset in capturing localized GW variations due to its coarse resolution. The statistical correlation analysis, integrating both climatic indices and model

results, highlighted several key findings: i) GW fluctuations resulted to be closely related to recharge and evapotranspiration patterns with a very large effect size association; ii) a small positive association was detected between GW levels and both ONI and SPEI values suggesting that climate cycles influence in minor extent the GW availability; iii) the relationship between SW (Atlantic Ocean and tidal channels) and the GW system significantly varied over the simulation, with an increasing contribution of SW inflow that could potentially increase the salinization risk. Furthermore, the developed methodology provides tools for the study of groundwater resources in other coastal areas of Patagonia and the world that face similar water problems. Even if the results obtained provide relevant information on water resource management in a coastal region, correlations observed between climate and GW systems should not be interpreted as direct relationships without additional analysis.

CRediT authorship contribution statement

Mattia Gaiolini: Writing – original draft, Software, Methodology, Investigation, Formal analysis, Data curation, Conceptualization. **Rosario Acosta:** Writing – review & editing, Methodology, Investigation, Formal analysis. **Eleonora Carol:** Writing – review & editing, Validation, Resources, Investigation. **Nicolò Colombani:** Writing – review & editing, Validation, Supervision, Software, Resources, Conceptualization.

Declaration of competing interest

The authors declare that they have no known competing financial interests or personal relationships that could have appeared to influence the work reported in this paper.

Data availability

Data will be made available on request.

References

Amanambu, A.C., Obarein, O.A., Mossa, J., Li, L., Ayeni, S.S., Balogun, O., Oyebamiji, A., Ochege, F.U., 2020. Groundwater system and climate change: present status and future considerations. J. Hydrol. 589, 125163. https://doi.org/10.1016/j.jhydrol.2020.125163.

Archer, D.R., Fowler, H.J., 2004. Spatial and temporal variations in precipitation in the Upper Indus Basin, global teleconnections and hydrological implications. Hydrol. Earth Syst. Sci. 8 (1), 47–61. https://doi.org/10.5194/hess-8-47-2004.

Balacco, G., Alfio, M.R., Fidelibus, M.D., 2022. Groundwater drought analysis under data scarcity: the case of the Salento aquifer (Italy). Sustainability 14 (2), 707. https://doi.org/10.3390/su14020707.

Bănăduc, D., Simić, V., Cianfaglione, K., Barinova, S., Afanasyev, S., Öktener, A., McCall, G., Simic, S., Curtean-Bănăduc, A., 2022. Freshwater as a sustainable resource and generator of secondary resources in the 21st century: stressors, threats, risks, management and protection strategies, and conservation approaches. Int. J. Environ. Res. Publ. Health 19 (24), 16570. https://doi.org/10.3390/ijerph192416570.

Bohn, V.Y., Rivas, R., Varni, M., Piccolo, M.C., 2020. Using SPEI in predicting water table dynamics in Argentinian plains. Environ. Earth Sci. 79, 1–16. https://doi.org/10.1007/s12665-020-09210-0.

Carol, E., Perdomo, S., Alvarez, M.D.P., Tanjal, C., Bouza, P., 2021. Hydrochemical, isotopic, and geophysical studies applied to the evaluation of groundwater salinization processes in quaternary beach ridges in a semiarid coastal area of northern Patagonia, Argentina. Water 13 (24), 3509. https://doi.org/10.3390/w13243509.

Carol, E., Perdomo, S., Tanjal, C., Scivetti, N., del Pilar Alvarez, M., 2024. Quaternary climatic events as conditioning factors of hydrogeologic characteristics and salinity in costal aquifers at northern Patagonia, Argentina. Quat. Res. 119, 152–161. https://doi.org/10.1017/qua.2023.72.

Chen, P.Y., Popovich, P.M., 2002. Correlation: Parametric and Nonparametric Measures, vol. 139. Sage.

Chiang, E., 2022. User guide for processing Modflow version 11 - a graphical user interface for MODFLOW, gsflow, modpath, MT3D, pest, seawat, and ZoneBudget. Simcore Software 1, 1–300. https://www.simcore.com/files/pm/v11/pm11.0.3pdf.

Cohen, J., Cohen, P., West, S.G., Aiken, L.S., 2003. Applied Multiple Regression/correlation Analysis for the Behavioral Sciences, third ed. Lawrence Erlbaum Associates, Mahwah, NJ. https://doi.org/10.4324/9780203774441.

Colombani, N., Gaiolini, M., Busico, G., Postacchini, M., 2021. Quantifying the impact of evapotranspiration at the aquifer scale via groundwater modelling and MODIS data. Water 13 (7), 950. https://doi.org/10.3390/w13070950.

Compagnucci, R., Araneo, D., 2007. Alcances de El Niño como predictor del caudal de los ríos andinos argentinos. Ing. Hidraul. Mex. 22 (3), 23–35. https://revistatyca.org.mx/index.php/tyca/article/view/177.

Dasgupta, B., Sanyal, P., 2022. Linking land use land cover change to global groundwater storage. Sci. Total Environ. 853, 158618. https://doi.org/10.1016/j.scitotenv.2022.158618.

Davey, M.K., Brookshaw, A., Ineson, S., 2014. The probability of the impact of ENSO on precipitation and near-surface temperature. Clim. Risk Manage. 1, 5–24. https://doi.org/10.1016/j.crm.2013.12.002.

Feng, W., Longuevergne, L., Kusche, J., Liang, S., Zhang, Y., Scanlon, B.R., Shum, C.K., Yeh, P.J.F., Long, D., Cao, G., Zhong, M., Xu, H., Xia, J., 2017. Groundwater storage variations in the North China Plain using multiple space geodetic observations. AGU Fall Meeting Abstracts 2017, G53B, 04.

Ferguson, G., Gleeson, T., 2012. Vulnerability of coastal aquifers to groundwater use and climate change. Nat. Clim. Change 2 (5), 342–345. https://doi.org/10.1038/nclimate1413.

Foster, S., Chilton, J., Nijsten, G.J., Richts, A., 2013. Groundwater—a global focus on the 'local resource'. Curr. Opin. Environ. Sustain. 5 (6), 685–695. https://doi.org/10.1016/j.cosust.2013.10.010.

Fucks, E., Charó, M., Pisano, F., 2012. Aspectos estratigráficos y geomorfológicos del sector oriental patagónico bonaerense. Rev. Soc. Geol. Esp. 25 (1–2), 29–44.

Grimm, A.M., Barros, V.R., Doyle, M.E., 2000. Climate variability in southern south America associated with el Niño and La Niña events. J. Clim. 13, 35–58. https://doi.org/10.1175/1520-0442(2000)013<0035:CVISSA>2.0.CO;2.

Harbaugh, A.W., 2005. MODFLOW-2005, the US geological survey modular ground-water model: the ground-water flow process. U.S. Geological Survey Techniques and Methods 6-A16; US Department of the Interior. US Geological Survey, Reston, VA, USA, p. 253. https://doi.org/10.3133/tm6A16.

Holman, I.P., Allen, D.M., Cuthbert, M.O., Goderniaux, P., 2012. Towards best practice for assessing the impacts of climate change on groundwater. Hydrogeol. J. 20 (1), 1.

IGN, 2024. Instituto Geográfico nacional. Available online: https://www.ign.gob.ar/NuestrasActividades/Geodesia/ModeloDigitalElevaciones/Introduccion.

INTA, 2024. Instituto Nacional de Tecnología Agropecuaria. Sistema de Información y Gestión Agrometeorológico de INTA. http://siga.inta.gob.ar/#/.

INTA, 2024. In: Rodríguez, Darío, Schulz, Guillermo, Moretti, Lucas (Eds.), Carta de suelos de la República Argentina: partido de Patagones, provincia de Buenos Aires. Ediciones INTA, Instituto de Suelos, p. 131, 2024.

Isla, F.I., 2017. Coastal barriers from Argentina: Buenos Aires, Patagonia and Tierra del Fuego. Quat. Environ. Geosci. 7 (1), 1–9.

Joshi, N., Kalra, A., 2021. Analyzing the association between ENSO and groundwater rise in the south atlantic-gulf region in the southeastern United States. Hydrol. 8 (3), 119. https://doi.org/10.3390/hydrology8030119.

Kamali, S., Asghari, K., 2023. The effect of meteorological and hydrological drought on groundwater storage under climate change scenarios. Water Resour. Manag. 37 (8), 2925–2943. https://doi.org/10.1007/s11269-022-03268-0.

Kayano, M.T., Andreoli, R.V., 2007. Relations of south American summer rainfall interannual variations with the pacific decadal oscillation climatol. Int. J. Climatol. 27, 531–540. https://doi.org/10.1002/joc.1417.

Kumar, C.P., 2012. Climate change and its impact on groundwater resources. Int. J. Eng. Sci. 1 (5), 43–60. https://www.jstor.org/stable/24092675.

Kuss, A.J.M., Gurdak, J.J., 2014. Groundwater level response in US principal aquifers to ENSO, NAO, PDO, and AMO. J. Hydrol. 519, 1939–1952. https://doi.org/10.1016/j.jhydrol.2014.09.069.

Li, B., Zhou, W., Zhao, Y., Ju, Q., Yu, Z., Liang, Z., Acharya, K., 2015. Using the SPEI to assess recent climate change in the yarlung zangbo river basin, south tibet. Water 7, 5474–5486. https://doi.org/10.3390/w7105474.

Lo, M.H., Famiglietti, J.S., Yeh, P.F., Syed, T.H., 2010. Improving parameter estimation and water table depth simulation in a land surface model using GRACE water storage and estimated base flow data. Water Resour. Res. 46 (5). https://doi.org/10.1029/2009WR007855.

Malki, M., Bouchaou, L., Hirich, A., Brahim, Y.A., Choukr-Allah, R., 2017. Impact of agricultural practices on groundwater quality in intensive irrigated area of Chtouka-Massa, Morocco. Sci. Total Environ. 574, 760–770. https://doi.org/10.1016/j.scitotenv.2016.09.145.

Mammoliti, E., Fronzi, D., Mancini, A., Valigi, D., Tazioli, A., 2021. WaterbalANce, a WebApp for thornthwaite–mather water balance computation: comparison of applications in two European watersheds. Hydrol. 8 (1), 34. https://doi.org/10.3390/hydrology8010034.

Mastrocicco, M., Colombani, N., 2021. The issue of groundwater salinization in coastal areas of the mediterranean region: a review. Water 13 (1), 90. https://doi.org/10.3390/w13010090.

Mercau, J.L., Nosetto, M.D., Bert, F., Giménez, R., Jobbágy, E.G., 2016. Shallow groundwater dynamics in the Pampas: climate, landscape and crop choice effects. Agric. Water Manag. 163, 159–168. https://doi.org/10.1016/j.agwat.2015.09.013.

McStraw, T.C., Pulla, S.T., Jones, N.L., Williams, G.P., David, C.H., Nelson, J.E., Ames, D. P., 2022. An open-source web application for regional analysis of GRACE groundwater data and engaging stakeholders in groundwater management. JAWRA J. Am. Water Resour. Assoc. 58 (6), 1002–1016. https://doi.org/10.1111/1752-1688.12968.

Misseri, L., Cellone, F., Bouza, P., Alvarez, M.P., Carol, E., 2020. Geohidrología de un sector de la marisma de Bahía San Blas. Rev. Mus. La Plata 5 (2), 500–509.

Mishra, R.K., 2023. Fresh water availability and its global challenge. Br. J. Multidiscip. Adv. Stud. 4 (3), 1–78. https://doi.org/10.37745/bjmas.2022.0208.

Navarro Céspedes, J.M., Hernández Anguiano, J.H., Alcántara Concepción, P.C., Dominguez Sarmiento, C., Morales Martínez, J.L., Knappett, P.S., Acosta Reyes, M. A., Li, Y., González, V.P., Zha, X., 2024. Influence of climate variability on change in storage of overexploited aquifers in a semi-arid region. Theor. Appl. Climatol. 155 (3), 2087–2103. https://doi.org/10.1007/s00704-023-04749-x.

Niswonger, R.G., Panday, S., Ibaraki, M., 2011. MODFLOW-NWT, a Newton formulation for MODFLOW-2005. US Geological Survey Techniques and Methods 6 (A37), 44. http://pubsdata.usgs.gov/pubs/tm/tm6a37/index.html.

Oude Essink, G.H., Van Baaren, E.S., De Louw, P.G., 2010. Effects of climate change on coastal groundwater systems: a modeling study in The Netherlands. Water Resour. Res. 46 (10). https://doi.org/10.1029/2009WR008719.

Pedoja, K., Regard, V., Husson, L., Martinod, J., Guillaume, B., Fucks, E., Iglesias, M., Weill, P., 2011. Uplift of Quaternary shorelines in eastern Patagonia: Darwin revisited. Geomorphology 127 (3–4), 121–142. https://doi.org/10.1016/j.geomorph.2010.08.003.

Piacentini, R.D., Valle Seijo, M.F., Pani, A., 2024. Impact of ENSO events and climate change on soil drying. Dry. Technol. 1–2. https://doi.org/10.1080/07373937.2024.2365120.

Rasouli, K., Scharold, K., Mahmood, T.H., Glenn, N.F., Marks, D., 2020. Linking hydrological variations at local scales to regional climate teleconnection patterns. Hydrol. Process. 34 (26), 5624–5641. https://doi.org/10.1002/hyp.13982.

Rateb, A., Scanlon, B.R., Pool, D.R., Sun, A., Zhang, Z., Chen, J., Clark, B., Faunt, C.C., Haugh, C.J., Hill, M., Hobza, C., McGuire, V.L., Reitz, M., Schmied, H.M., Sutanudjaja, E.H., Swenson, S., Wiese, D., Xia, Y., Zell, W., 2020. Comparison of groundwater storage changes from GRACE satellites with monitoring and modeling of major US aquifers. Water Resour. Res. 56 (12). https://doi.org/10.1029/2020WR027556.

Rostami, K., Peltier, W.R., Mangini, A., 2000. Quaternary marine terraces, sea-level changes and uplift history of Patagonia, Argentina: comparisons with predictions of the ICE-4G (VM2) model of the global process of glacial isostatic adjustment. Quat. Sci. Rev. 19 (14–15), 1495–1525. https://doi.org/10.1016/S0277-3791(00)00075-5.

Rutter, N., Radtke, U., Schnack, E.J., 1990. Comparison of ESR and amino acid data in correlating and dating Quaternary shorelines along the Patagonian coast, Argentina. J. Coast Res. 391–411. https://www.jstor.org/stable/4297690.

Saito, L., Christian, B., Diffley, J., Richter, H., Rohde, M.M., Morrison, S.A., 2021. Managing groundwater to ensure ecosystem function. Groundwater 59 (3), 322–333. https://doi.org/10.1111/gwat.13089.

Scanlon, B.R., Keese, K.E., Flint, A.L., Flint, L.E., Gaye, C.B., Edmunds, W.M., Simmers, I., 2006. Global synthesis of groundwater recharge in semiarid and arid regions. Hydrol. Process. 20 (15), 3335–3370. https://doi.org/10.1002/hyp.6335.

Scanlon, B.R., Fakhreddine, S., Rateb, A., de Graaf, I., Famiglietti, J., Gleeson, T., Grafton, R.Q., Jobbagy, E., Kebede, S., Kolusu, S.R., Konikow, L.F., Long, D., Mekonnen, M., Müller Schmied, H., Mukherjee, A., MacDonald, A., Reedy, R.C., Shamsudduha, M., Simmons, C.T., Sun, A., Taylor, R.G., Villholth, K.G., Vörösmarty, C.J., Zheng, C., 2023. Global water resources and the role of groundwater in a resilient water future. Nat. Rev. Earth Environ. 4 (2), 87–101. https://doi.org/10.1038/s43017-022-00378-6.

Scordo, F., Perillo, G.M., Cintia Piccolo, M., 2018. Effect of southern climate modes and variations in river discharge on lake surface area in Patagonia. Inland Waters 8 (3), 341–355. https://doi.org/10.1080/20442041.2018.1487118.

Secci, D., Tanda, M.G., D'Oria, M., Todaro, V., Fagandini, C., 2021. Impacts of climate change on groundwater droughts by means of standardized indices and regional climate models. J. Hydrol. 603, 127154. https://doi.org/10.1016/j.jhydrol.2021.127154.

Shayeghi, A., Ziveh, A.R., Bakhtar, A., Teymoori, J., Hanel, M., Godoy, M.R.V., Markonis, Y., AghaKouchak, A., 2024. Assessing drought impacts on groundwater and agriculture in Iran using high-resolution precipitation and evapotranspiration products. J. Hydrol. 631, 130828. https://doi.org/10.1016/j.jhydrol.2024.130828.

Srivastav, A.L., Dhyani, R., Ranjan, M., Madhav, S., Sillanpää, M., 2021. Climate-resilient strategies for sustainable management of water resources and agriculture. Environ. Sci. Pollut. Res. 28 (31), 41576–41595. https://doi.org/10.1007/s11356-021-14332-4.

Sun, A.Y., Green, R., Swenson, S., Rodell, M., 2012. Toward calibration of regional groundwater models using GRACE data. J. Hydrol. 422, 1–9. https://doi.org/10.1016/j.jhydrol.2011.10.025.

Vargas, W., Peñalba, O.C., Minettmi, J.L., 1999. Las precipitaciones mensuales en zonas de la Argentina y el ENSO. Un enfoque hacia problemas de decisión Meteorológica 24, 3–22.

Vargas, W.M., Minetti, J.L., Poblete, A.G., 2002. Low frequency oscillations in climatic and hydrological variables in southern South America's tropical subtropical regions. Theor. Appl. Climatol. 72, 29–40.

Vicente-Serrano, S.M., Beguería, S., Lopez-Moreno, J.I., 2010. A multi-scalar drougth index sensitive to global warming: the Standarized Precipitation Evapotranspiration Index – SPEI. J. Clim. 23, 1696–1718. https://doi.org/10.1175/2009JCLI2909.1.

Vicente-Serrano, S.M., Beguería, S., 2016. SPEI global drougth monitor. http://sac.csic.es/spei/home.html.

Yang, S., Li, Z., Yu, J.Y., Hu, X., Dong, W., He, S., 2018. El niño–southern oscillation and its impact in the changing climate. Natl. Sci. Rev. 5 (6), 840–857. https://doi.org/10.1093/nsr/nwy046.

Zhou, Y., Li, W., 2011. A review of regional groundwater flow modeling. Geosci. Front. 2, 205–214. https://doi.org/10.1016/j.gsf.2011.03.003.